Estimated Displacements for the VLBI Reference Point of the DSS 13 26-m Antenna

H. McGinness, G. Gale, and R. Levy
DSN Engineering Section

It is shown that the displacement of the defined reference point caused by bearing runout, temperature change, and wind loading, under expected environmental conditions, will not exceed a few millimeters.

I. Introduction

One of the tasks associated with the very long base interferometry (VLBI) project is the estimation of the displacements of the reference point of the 26-m antenna at DSS 13. This antenna is of the azimuth-elevation type, and its reference point is defined as a point on the azimuth axis at the level of the elevation axis. The desired displacements are the horizontal and vertical displacements of the reference point, with respect to the ground, caused by azimuth bearing runout, wind, and temperature variations.

At first it was believed that these displacements could be obtained by placing a target near the reference point and observing it with two theodolites spaced 90 degrees about the antenna azimuth axis as shown in Fig. 1. Experiments made with a 1/48 scale model of the antenna indicated that the reference point target could be seen from theodolites located as shown in Fig. 1 and that displacements caused by bearing runout, wind, and temperature changes could be observed. Concrete monuments were placed as indicated in the figure and theodolites mounted on them. It was then realized that the antenna was different enough from the model to prevent the target from being seen at many azimuth positions, thus making the proposed bearing runout test impossible.

Three attempts were made to measure the vertical and horizontal displacements caused by temperature gradients. The antenna was parked and theodolite readings made at various times of the day. On one windless day, when the ambient temperature ranged from 43°C at hour 1530 to 21°C at hour 0700, both theodolites showed an azimuth change of 2 arc seconds. The corresponding horizontal resultant displacement is 0.56 mm. The changes in the theodolite elevation angles during this time were 26 and 33 arc seconds. These elevation changes are not only much more than was anticipated for such a temperature change, but the signs of both angular changes are wrong in that the reference point seems to be highest at the lowest ambient temperature! This paradox may be explained by vertical temperature gradients in the air affecting its refractive properties. Another possible explanation is that the distances between the reference point and the theodolite monuments increase slightly as the ambient increases, thus producing smaller elevation angles. Neither of these hypotheses would affect the azimuth angle changes. Therefore, it seems proper to accept the measured azimuth angle changes, but to consider

the elevation changes as spurious. It was necessary to develop other methods for obtaining the reference point displacements.

The methods employed for these measurements are discussed as follows:

(1) Horizontal displacement from bearing runout.

(2) Displacement caused by wind loading.

(3) Vertical displacement from temperature change.

II. Horizontal Displacement from Bearing Runout

The horizontal displacement of the reference point caused by runout of the antenna azimuth bearings was calculated from a set of runout measurements taken at a point near ground level and a set of clinometer measurements taken at the top of the alidade. The runout measurements were made by utilizing a device curiously called the "magic tee." Figure 2 shows the position of this device, the purpose of which is to transmit the azimuth displacement of the antenna dish (the dish elevation bearings) to the azimuth encoder mounted on a pedestal near the ground. As designed, the device transmits the azimuth displacement without distortion.

Preparation for the test consisted of the removal of the azimuth encoder, drilling and reaming for and insertion of two taper pins through the lower guide bearing flange and the encoder pedestal, dropping the vertical leg of the magic tee 3 mm by turning the nut at its center support by 1-1/2 turns, thus allowing the lower guide bearing to drop away from the encoder pedestal structure, and installing three equally spaced struts between the magic tee and alidade kingpost. The lower end of the magic tee was now free from any external constraint and rigidly connected to the alidade, yet could be restored exactly to its original configuration. Since the azimuth encoder was gone, a cardboard chart with 10-degree angular marks was placed in the encoder pedestal just below the end of the magic tee. A stylus clamped to the magic tee completed the temporary azimuth angle contrivance. The installation of two dial indicators, one on the east side and one on the south side, and the placement of two levels (clinometers) shown in Fig. 2 completed the preparation. The cylindrical surface of the magic tee touching the dial indicators had been measured and found to be truly circular.

If the azimuth bearings were perfect, the dial indicator readings plotted versus the azimuth angle would be perfect sinusoids, the amplitudes corresponding to the distance that the center of the circular surface was offset from the centerline of the perfect azimuth bearings. The phase angle between the two sinusoids would be 90 degrees since the two dial indicators were 90 degrees apart. Similarly, if the azimuth bearings were perfect, the level readings plotted against the azimuth angle would produce perfect sinusoids, the amplitude corresponding to the amount that the bearing centerline was off vertical. The phase angle would also be 90 degrees because the levels were 90 degrees apart. The true runout of the lower end of the magic tee is the difference between the curve plotted from the dial indicator readings and the fictitious perfect sinusoid. The fictitious sinusoid can be approximated closely by best fitting a sinusoid to the experimentally derived curve. The difference between the best fitted sinusoid and the experimental curve is a good approximation to the true bearing runout at the lower end of the magic tee. Similarly, the angular change in the position of the vertical axis is the difference between the best fitted sinusoid of the clinometer readings and the actual clinometer readings.

The horizontal runout at the reference point was calculated as follows:

The curves of Fig. 3 were plotted by considering compression of the dial indicators to be positive. The variations of the measured points from the best fitted sinusoids, δ_E and δ_S, are defined as positive as shown in Fig. 3. These are the runouts at the lower end of the magic tee.

The curves of Fig. 4 were plotted by considering clinometer "a" reading positive when its "W" end went downward and clinometer "b" reading positive when its "n" end went downward. The variations of the measured points from the best fitted sinusoids, θ_a and θ_b, are defined as positive as shown in Fig. 4. These are the angular changes in the position of the vertical axis, and each is a function of the antenna azimuth angle ψ.

Consider a view of the bearing axis when looking northward. The angular change of the bearing axis as seen in this view, θ_{EW}, is:

$$\theta_{EW} = \theta_a \cos \psi - \theta_b \sin \psi \qquad (1)$$

The positive direction of θ_{EW} is when the upper end of the bearing axis is tilted to the west. Consider a view of the bearing axis when looking eastward. The angular change of the bearing axis as seen in this view, θ_{NS}, is:

$$\theta_{NS} = \theta_b \cos \psi + \theta_a \sin \psi \qquad (2)$$

The positive direction of θ_{NS} is when the upper end of the bearing axis is tilted to the north.

At the reference point the horizontal displacements to the east and to the south are δ_{RE} and δ_{RS}, respectively:

$$\delta_{RE} = \delta_E - \ell\theta_{EW} \tag{3}$$

$$\delta_{RS} = \delta_S - \ell\theta_{NS} \tag{4}$$

where ℓ is the vertical distance from the dial indicators to the reference point. Its numerical value is 8.5 m as shown in Fig. 2.

The substitution of (1) and (2) into (3) and (4), respectively, yields the following:

$$\delta_{RE} = \delta_E - \ell[\theta_a \cos\psi - \theta_b \sin\psi] \tag{5}$$

$$\delta_{RS} = \delta_S - \ell[\theta_b \cos\psi + \theta_a \sin\psi] \tag{6}$$

which are, respectively, the east and south components of the horizontal displacement at the reference point caused by azimuth bearing runout. The resultant horizontal runout, δ_T, is:

$$\delta_T = \sqrt{\delta_{RE}^2 + \delta_{RS}^2} \tag{7}$$

Dial indicator and clinometer readings were taken for six complete turns of the antenna. In all instances the wind was near zero and the weather was sunny. The elevation angle was 30 degrees for four runs and 4.7 degrees and 60.2 degrees for the other two runs. It was observed that the instrument readings were not affected by a change in elevation angle. The readings from two typical runs are plotted in Figs. 3 and 4. The values of δ_E, δ_S, θ_a, and θ_b were read from these plots and are tabulated in Table 1 as a function of the antenna azimuth angle ψ. Then the total horizontal displacement at the reference point, δ_T, was calculated using Eqs. (5), (6), and (7), and the results entered in the last column of Table 1. The largest entry in the δ_T column is 0.782 mm, which represents the maximum horizontal displacement at the reference point caused by runout of the antenna azimuth bearings.

A corroborative check was made by attaching a pencil to the lower end of the magic tee so that its point was bearing against a paper fixed to the encoder pedestal. The antenna was rotated 360 degrees and the pencil trace compared to a perfect circle. The maximum discrepancy appeared to be approximately 0.50 mm, which agrees with the maximum values of δ_E and δ_S of Table 1. It was observed that the center of the angle chart serving as a temporary azimuth indicator was displaced 6.35 mm from the center of the antenna rotation. True antenna azimuth angles were calculated to correspond to the indicated angles on the chart, and these true angles were used in plotting Figs. 3 and 4.

III. Displacements Caused by Wind

A finite element model is available to estimate displacements at a set of nodal points of the DSS 13 26-m antenna mount. In addition to nodes of the mount, the model contains one node simulating the reflector vertex. The model, a source program to perform analysis, and input wind loading data for a spectrum of antenna attitudes relative to the wind direction are preserved on tape. The defined reference point is approximately halfway between two nodes, and its displacement may be taken as the mean displacement of these two nodes.

In order to check the accuracy of the analysis regarding the horizontal displacement of the elevation bearings, an experiment was made. As shown in Fig. 5, steel cables of 16-mm diameter were attached to the antenna near each elevation bearing and connected to a large truck by means of a snatch block. The truck was parked with its rear wheels in a ditch about 50 m south of the antenna. A cable jack and force scale were connected into the cable as shown in Fig. 5. Figure 6 shows the position of the eye bolts through which the free ends of the cables were looped and clamped. Each eye bolt was approximately 25 cm from the center of the elevation bearing and was attached to a 1.27-cm thick plate near a corner welded to heavy sections, thus insuring that local deflections would be negligible. A controlled force was applied by the jack.

The deflection of one of the eye bolts was measured by the device shown in Fig. 5. A 1.6-mm diameter steel cable was attached to the west eye bolt, extended 38 m southward, passed over a 15-cm diameter pulley mounted in a plywood bracket, and attached to a 23-kg steel mass. From the bottom of the steel mass was suspended the piston of the displacement gage as is shown in Fig. 7. Kerosene was poured into the glass cylinder to an appropriate level. The relationship between the downward displacement of the piston, Y_P, and the upward displacement of the liquid level, Y_L, is:

$$Y_L = \frac{d^2}{D^2 - d^2} Y_P \tag{8}$$

For the dimensions shown in Fig. 7, $d^2/(D^2 - d^2)$ is 15.226; thus the device magnifies the piston displacement by this amount and makes small piston displacements easy to measure.

A jack force of 40,000 newtons was applied to the cable. It was observed that the angle between the cable and the hori-

zontal was approximately 7.5 degrees. The small cable to the 23-kg mass made an angle of 9.5 degrees with the horizontal. The lowest point of the liquid level was marked on the glass cylinder, and then the jack was operated to remove the cable force. It is estimated that the load was removed within a minute. The lowest point of the liquid level was marked immediately and measured. It had lowered by 7.62 mm (0.30 in.). It is believed that the measurement is accurate to within 0.75 mm.

The horizontal force applied near each elevation bearing was 40,000 X cos 7.5 degrees or 39,658 newtons. The horizontal deflection at the west elevation bearing was (7.72/15.226) cos 9.5 degrees or 0.514 mm. According to the structural analysis, a horizontal force of 39,658 newtons applied horizontally at each elevation bearing would produce a horizontal displacement of 0.546 mm, which is approximately the measured amount. Therefore, it seems that the pedestal and alidade structures were successfully modeled in the structural analysis and that the analysis may reliably be employed to predict any displacements caused by wind loading.

This test was conducted on August 28, 1978. The wind speed was less than 2.23 meters per second (5 mph) and the weather was sunny.

Figure 8 shows calculated displacements at the antenna reference point. Both the X component (the horizontal displacement perpendicular to the elevation axis) and the resultant magnitude are shown as functions of the wind azimuth angle and antenna elevation angle. Since the above described experiment verified the analysis on which these curves are based, it is believed these curves are reliable. Displacement at other wind speeds can be determined by considering the displacements proportional to the square of the wind speed.

Figure 9 shows the calculated displacements at the antenna vertex, due to the flexibility of the antenna pedestal and alidade structure, under a 14.14-meter per second wind loading.

The curves of Figs. 8 and 9 were plotted from the data listed in Table 2, which are the displacement components for various elevation and azimuth angles.

IV. Vertical Displacement from Temperature Changes

Experiments made with the displacement gages, as shown in Fig. 7, indicated that they would serve well for measuring the vertical displacement of each end of the alidade. The experiments consisted of moving the piston a known amount and measuring the vertical excursion of the lowest point of the fluid level. Because of capillary effects, the fluid height was not constant. By moving the piston horizontally until it touched the glass cylinder, the liquid on the opposite side would be at the lowest level. Many trials showed that the displacement magnification obtained experimentally was essentially the same as that calculated by Eq. (8).

The vertical displacement at the reference point would be the mean of the displacements at the alidade ends, provided there was no bowing or warpage of the alidade. Figure 10 shows the test setup. Three pairs of active and dummy displacement gages were disposed as shown in the figure. Figure 11 is a photograph of a pair of the displacement gages. The purpose of the dummy gage was to allow for evaporation and thermal expansion of the liquid (kerosene), since the test would last for many hours. In order to account for any bowing of the alidade, a displacement gage was placed between the center of the alidade and a taut cable stretched between the elevation bearings. The cable was kept taut by being passed over a pulley clamped to one elevation bearing and loaded by a dead weight. Since the elevation bearings are near the alidade ends, it may be assumed that the displacement of the bearings is essentially the same as the end displacements.

The other two pairs of displacement gages were put on steel blocks leveled against the pavement directly beneath the alidade ends. Steel angles were temporarily bolted to the upper surface of the alidade and the 1.00-mm diameter Invar A36 wire clamped to the angles. The lower ends of the wires were attached to the gage pistons as shown in Fig. 7. A downward force of approximately 125 newtons was applied to each piston to insure that the wire was yielded to a straight condition. Kerosene was put into all gage units. Each dummy unit was adjusted so that the amount of kerosene below its piston approximately matched that in the corresponding active gage. Also, the liquid levels of the dummy and active gages were approximately matched. Thus, both the evaporation and thermal expansion effects would be matched at each pair of gages.

The first test was begun on September 11, 1968 at hour 1630. Five sets of readings were taken during the 15-hour period that the antenna was stationary at zero azimuth and 5-degree elevation. The results are listed in Table 3 from which it may be seen that there was no relative displacement between the active and reference gages at the top center of the alidade. Thus, there was no bowing of the alidade over the ambient temperature range from 33.3 to 21.8°C. This indicates that the mean of the vertical displacements at the east and west ends of the alidade would represent the vertical displacement of the defined reference point. During this test the wind was less than 2 meters per second and the sky was clear.

A subsequent test was begun on October 13, 1978 when there was an opportunity to record data for two consecutive days with the antenna parked at zero azimuth and 45-degree elevation. Only the east and west displacement gages were installed at this time, since the previous test had established that there was no bowing of the alidade structure. The results are listed in Table 4. With one exception the readings were taken at approximately 3-hour intervals. The displacement at a gage is proportional to the relative displacement between the active and dummy gage. These relative displacements were divided by the magnification factor of the gages, namely, 15.23, averaged, and plotted versus time as shown in Fig. 12. Also shown in the figure are the ambient air temperature and the mean temperature of the two thermometers mounted on the pedestal structural members. Under the assumption that the Invar wire supporting the active gage has a zero coefficient of expansion, the displacement curve of Fig. 12 gives directly the vertical displacement of the antenna reference point during the 48-hour test. The total excursion over this period was 0.525 mm. The ambient air temperature range was 17°C, and the mean thermometer reading range was 8.6°C. The inside of the pedestal is air conditioned, and this partially accounts for the large difference between the two temperature ranges.

Actually, the Invar wire has a finite expansion coefficient, which is about 1/11 that of steel. Also, the temperature of the small diameter Invar wire is likely to be very close to the ambient air temperature. Since the ambient range was approximately twice that of the measured steel temperature range, the vertical displacement of the reference point is likely to be 2/11 more than the curve of Fig. 12 shows. Therefore, over the test period of 48 hours, a better estimate of the total vertical excursion of the reference point is 0.62 mm.

The vertical displacement of the reference point, δ_v, may be expressed as follows:

$$\delta_v = \ell \, \alpha \, \Delta T \tag{9}$$

where ℓ is the effective height of the steel structure, α is the expansion coefficient of steel, and ΔT is the average temperature change.

Taking $\ell = 9000$ mm, $\delta_v = 0.62$ mm, and $\alpha = 11 \times 10^{-6}$ per degree C, and solving for ΔT, there is obtained: $\Delta T = 6.26°C$, which is appreciably less than the mean thermometer reading range of 8.6°C. This suggests that the average temperature of the steel structure did not change as much as the two thermometers indicated.

It would appear that with the air conditioning system currently in use, the effective diurnal temperature change of the steel pedestal and alidade is less than half the diurnal ambient temperature change.

V. Conclusions

The displacements of the defined antenna reference point will not exceed the following values:

(1) 0.782-mm horizontal component caused by runout of the azimuth bearings.

(2) 1.00-mm horizontal component caused by a wind of 14.14 meters per second.

(3) 0.62-mm vertical component caused by an ambient air temperature change of 17°C.

Table 1. Experimental data for bearing runout

Azimuth angle ψ, deg	δ_E, mm	δ_S, mm	θ_a, mrad	θ_b, mrad	δ_{RE}, mm	δ_{RS}, mm	δ_T, mm
0	0.076	−0.076	0.003	−0.015	0.051	0.051	0.071
10	0.076	0	−0.020	−0.015	0.221	0.155	0.270
20	0.127	0.076	−0.020	−0.010	0.254	0.213	0.332
30	0.127	0.203	−0.045	−0.010	0.416	0.467	0.626
40	0	0.330	−0.039	0.015	0.330	0.444	0.554
50	−0.127	0.381	−0.040	0.012	0.170	0.574	0.599
60	−0.254	0.279	−0.040	0.035	0.152	0.424	0.451
70	−0.381	0.279	−0.040	0.030	−0.024	0.508	0.509
80	−0.305	0.254	−0.039	0.030	0.004	0.535	0.536
90	−0.432	0.508	−0.030	0.030	−0.175	0.762	0.782
100	−0.279	0.127	−0.028	0.025	−0.101	0.399	0.411
110	−0.127	−0.127	−0.025	0.010	−0.119	0.102	0.157
120	−0.228	−0.279	−0.025	0.010	−0.254	−0.053	0.260
130	−0.127	−0.381	−0.020	−0.015	−0.333	−0.333	0.471
140	0	−0.508	−0.029	−0.020	0.305	−0.480	0.569
150	0.254	−0.305	−0.026	−0.030	−0.066	0.025	0.071
160	0.279	−0.381	−0.030	−0.030	−0.076	−0.533	0.539
170	0.381	−0.254	−0.045	−0.030	−0.041	−0.432	0.434
180	0.279	−0.508	−0.050	−0.030	−0.148	−0.762	0.776
190	0.254	−0.203	−0.040	−0.025	−0.043	−0.353	0.356
200	0.305	0	−0.018	−0.020	0.218	−0.211	0.304
210	0.229	−0.076	−0.020	−0.010	0.122	−0.234	0.263
220	0.127	0	0.008	−0.010	0.234	−0.021	0.235
230	0	0.127	0.005	0	0.028	0.160	0.162
240	0	0.254	0.010	−0.005	0.079	0.307	0.317
250	−0.152	0.279	0.020	0	−0.094	0.439	0.449
260	−0.279	0.229	0.022	0.005	−0.287	0.419	0.508
270	−0.305	0.076	0.032	0.005	−0.348	0.348	0.492
280	−0.330	0.127	0.035	0	−0.381	0.419	0.566
290	−0.203	0.127	0.035	−0.005	−0.264	0.419	0.495
300	−0.102	0	0.033	−0.015	−0.130	0.307	0.333
310	−0.127	−0.127	0.030	−0.020	−0.160	−0.041	0.165
320	0	−0.127	0.030	−0.025	−0.058	0.201	0.209
330	0	−0.076	0.025	−0.030	−0.056	0.251	0.258
340	0.152	−0.127	0.030	−0.030	−0.0002	0.201	0.201
350	0.127	−0.051	0.030	−0.025	−0.086	0.203	0.221
360	0.228	−0.076	0	−0.025	0.229	0.135	0.265

Table 2. Computed wind loading displacements in millimeters for 14.14-m/s wind speed

Elevation angle, deg	Vertex				Reference point			
	N	A	S	$\sqrt{N^2+A^2+S^2}$	x	y	z	$\sqrt{x^2+y^2+z^2}$
	(a) Antenna azimuth with respect to wind = 0							
0	1.219	2.540	−0.003	2.817	0.937	−0.002	0.356	1.002
10	1.219	2.286	−0.007	2.590	0.864	−0.003	0.295	0.912
20	1.219	2.032	−0.003	2.370	0.838	0	0.244	0.873
30	1.219	1.803	0.007	2.177	0.762	0	0.203	0.789
40	1.193	1.575	0.012	1.976	0.711	−0.005	0.165	0.730
50	1.168	1.372	0.013	1.801	0.635	−0.008	0.142	0.651
60	1.118	1.194	0.009	1.635	0.584	−0.010	0.132	0.599
70	0.889	0.864	0.005	1.239	0.432	−0.008	0.117	0.447
80	0.685	0.864	−0.002	1.103	0.330	−0.005	0.109	0.348
90	0.483	0.330	−0.006	0.585	0.236	−0.001	0.117	0.264
	(b) Antenna azimuth with respect to wind = 30 degrees							
0	1.092	2.311	0.122	2.559	0.864	0.043	0.320	0.922
10	1.27	2.311	0.137	2.641	0.889	0.058	0.305	0.942
20	1.346	2.184	0.135	2.569	0.864	0.069	0.279	0.910
30	1.321	1.905	0.099	2.320	0.787	0.076	0.234	0.825
40	1.346	1.753	0.109	2.213	0.762	0.076	0.206	0.793
50	1.346	1.575	0.107	2.074	0.711	0.053	0.193	0.739
60	1.245	1.321	0.081	1.817	0.610	−0.007	0.175	0.634
70	0.965	0.914	0.064	1.331	0.457	−0.028	0.145	0.480
80	0.711	0.584	0.046	0.921	0.330	−0.033	0.130	0.356
90	0.533	0.381	0	0.655	0.254	−0.038	0.122	0.284
	(c) Antenna azimuth with respect to wind = 60 degrees							
0	0.914	1.880	0.124	2.094	0.686	0.071	0.254	0.735
10	1.067	1.956	0.196	2.236	0.737	0.081	0.254	0.783
20	1.118	1.803	0.170	2.128	0.711	0.043	0.241	0.752
30	1.118	1.600	0.069	1.953	0.660	0.0064	0.211	0.693
40	1.041	1.346	0.112	1.706	0.559	−0.051	0.173	0.587
50	0.863	0.991	0.102	1.318	0.457	−0.142	0.130	0.496
60	0.668	0.711	0.122	0.978	0.330	−0.160	0.091	0.378
70	0.483	0.457	0.107	0.673	0.241	−0.160	0.063	0.296
80	0.356	0.305	0.046	0.470	0.170	−0.145	0.053	0.230
90	0.216	0.147	−0.006	0.261	0.109	−0.130	0.053	0.178
	(d) Antenna azimuth with respect to wind = 90 degrees							
0	−0.056	−0.140	−0.117	0.191	−0.066	0.006	−0.017	0.068
10	0.036	0.025	−0.137	0.144	−0.020	−0.047	0.012	0.052
20	0.076	0.089	−0.102	0.155	0.002	−0.076	0.025	0.080
30	0.076	0.081	−0.051	0.122	0.005	−0.086	0.028	0.091
40	−0.023	−0.043	−0.014	0.051	−0.028	−0.091	0.005	0.096
50	−0.001	−0.013	0.008	0.015	−0.013	−0.097	0.011	0.098
60	0.084	0.074	0.025	0.114	0.022	−0.107	0.033	0.114
70	−0.010	−0.021	0.030	0.038	−0.011	−0.091	0.011	0.093
80	−0.104	−0.104	0.023	0.149	−0.046	−0.074	−0.012	0.088
90	−0.094	−0.091	0.005	0.131	−0.041	−0.063	−0.011	0.076

Table 2 (contd)

Elevation angle, deg	Vertex				Reference point			
	N	A	S	$\sqrt{N^2+A^2+S^2}$	x	y	z	$\sqrt{x^2+y^2+z^2}$
	(e) Antenna azimuth with respect to wind = 120 degrees							
0	−0.251	−0.533	0.356	0.689	−0.206	−0.058	−0.074	0.226
10	−0.246	−0.457	−0.279	0.590	−0.193	−0.097	−0.061	0.224
20	−0.254	−0.432	−0.193	0.537	−0.193	−0.132	−0.056	0.240
30	−0.305	−0.457	−0.099	0.558	−0.203	−0.152	−0.056	0.260
40	−0.381	−0.483	−0.043	0.616	−0.221	−0.185	−0.061	0.295
50	−0.431	−0.508	0.015	0.667	−0.231	−0.191	−0.066	0.307
60	−0.457	−0.483	0.036	0.666	−0.231	−0.188	−0.069	0.306
70	−0.432	−0.432	0.046	0.612	−0.211	−0.168	−0.066	0.277
80	−0.381	−0.330	0.030	0.505	−0.180	−0.150	−0.058	0.242
90	−0.254	−0.196	−0.006	0.321	−0.130	−0.130	−0.053	0.191
	(f) Antenna azimuth with respect to wind = 150 degrees							
0	−0.685	−1.448	−0.206	1.615	−0.533	−0.021	−0.201	0.570
10	−0.787	−1.422	−0.170	1.635	−0.533	−0.056	−0.196	0.571
20	−0.813	−1.295	−0.107	1.533	−0.533	−0.084	−0.180	0.569
30	−0.889	−1.270	−0.076	1.552	−0.508	−0.102	−0.178	0.548
40	−1.041	−1.295	−0.036	1.662	−0.533	−0.119	−0.206	0.584
50	−0.965	−1.067	−0.010	1.439	−0.457	−0.134	−0.185	0.511
60	−0.864	−0.889	−0.004	1.239	−0.406	−0.127	−0.163	0.456
70	−0.813	−0.762	−0.008	1.114	−0.381	−0.099	−0.147	0.420
80	−0.711	−0.584	0.006	0.920	−0.330	−0.061	−0.134	0.362
90	−0.558	−0.406	0	0.691	−0.279	−0.038	−0.122	0.307
	(g) Antenna azimuth with respect to wind = 180 degrees							
0	−0.668	−1.473	0	1.614	−0.584	0.001	−0.198	0.617
10	−0.762	−1.448	−0.006	1.636	−0.610	−0.004	−0.188	0.638
20	−0.889	−1.448	−0.023	1.699	−0.610	−0.012	−0.191	0.639
30	−1.117	−1.549	0.005	1.910	−0.635	−0.003	−0.218	0.672
40	−1.372	−1.702	−0.005	2.186	−0.711	−0.002	−0.254	0.755
50	−1.295	−1.422	−0.004	1.924	−0.635	−0.008	−0.241	0.679
60	−1.092	−1.092	−0.011	1.545	−0.508	−0.015	−0.208	0.549
70	−0.940	−0.838	−0.009	1.259	−0.432	0.012	−0.180	0.468
80	−0.737	−0.610	−0.006	0.956	−0.356	0.010	−0.145	0.385
90	−0.533	−0.406	−0.006	0.671	−0.254	−0.001	−0.114	0.279

Reference: RIL AZEL UPDATE, 08:26:33 Nov. 28, 1978

Table 3. Preliminary experimental data for thermal displacement

Date (1978)	Time	East gages, cm		West gages, cm		Top gages, cm		Pedestal temperature, °C		Average of north and south	Ambient temperature, °C
		Active	Reference	Active	Reference	Active	Reference	North	South		
Sept. 11	1630	4.60	4.50	4.35	5.05	5.50	5.80	26.53	27.78	27.15	33.3
	1900	4.35	4.40	3.35	4.75	5.10	5.40	25.56	24.72	25.14	27.5
	2100	3.90	4.40	3.20	4.60	5.00	5.30	23.89	23.33	23.61	26.4
	2300	3.80	4.30	3.20	4.50	5.00	5.30	23.61	23.61	23.61	24.2
Sept. 12	0600	3.90	4.30	3.30	4.40	4.95	5.30	22.78	23.33	23.05	21.8

Table 4. Experimental data for thermal displacement

Date (1978)	Time	East gages, cm		West gages, cm		Pedestal temperature, °C		Average of north and south	Ambient temperature, °C	Weather
		Active	Reference	Active	Reference	North	South			
Oct. 13	2100	4.50	4.75	6.15	5.00	26.94	26.67	26.81	19.83	Calm & clear
Oct. 14	0008	4.50	4.75	6.20	4.80	25.28	25.14	25.21	20.38	Calm & clear
	0330	4.40	4.70	6.40	4.80	22.22	22.78	22.50	16.05	Calm & clear
	0605	4.40	4.70	6.40	4.70	22.22	21.94	22.08	13.68	Calm & clear
	0900	5.00	5.40	6.90	4.85	23.89	24.17	24.03	26.58	Calm & clear
	1155	4.80	5.50	6.70	5.40	25.83	29.44	27.64	29.03	Calm & clear
	1500	4.40	5.00	6.90	5.90	29.17	32.08	30.63	30.45	Calm & clear
	1730	4.55	4.90	6.40	5.70	29.17	29.17	29.17	–	Calm, sundown
	2100	4.40	4.65	6.00	4.85	23.33	23.06	23.19	16.61	Clear, wind 5 m/s
Oct. 15	0002	4.45	4.65	6.25	4.85	23.06	23.33	23.19	18.51	Clear, wind 5 m/s
	0630	4.70	4.65	6.40	4.65	22.50	23.06	22.78	21.58	Before sunup, wind 5 m/s
	0900	4.75	4.75	6.65	4.70	23.06	23.61	23.33	24.07	Wind 7 m/s
	1200	4.90	4.90	6.40	4.90	24.72	26.39	25.56	26.85	Calm & bright
	1500	4.50	4.85	6.60	5.15	26.39	28.61	27.50	28.54	Calm & bright
	1730	4.45	4.70	6.25	5.10	27.50	28.06	27.78	26.29	Calm, sundown
	2100	4.40	4.60	5.95	4.55	24.17	23.61	23.89	22.58	Clear, wind 9 m/s

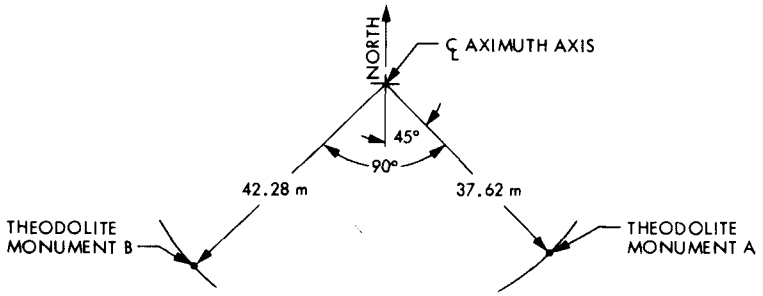

Fig. 1. Location of theodolite monuments

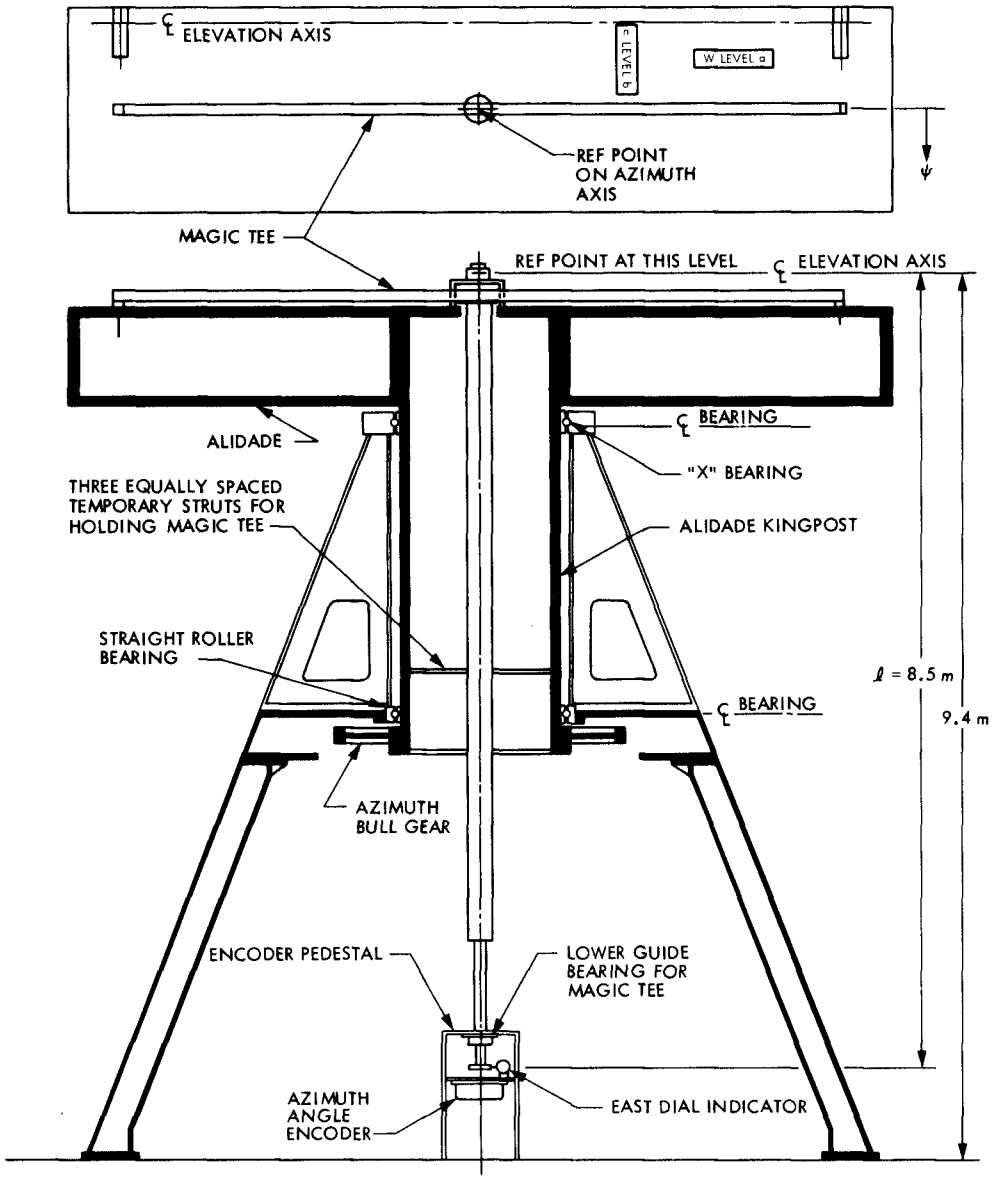

Fig. 2. Bearing runout instrumentation

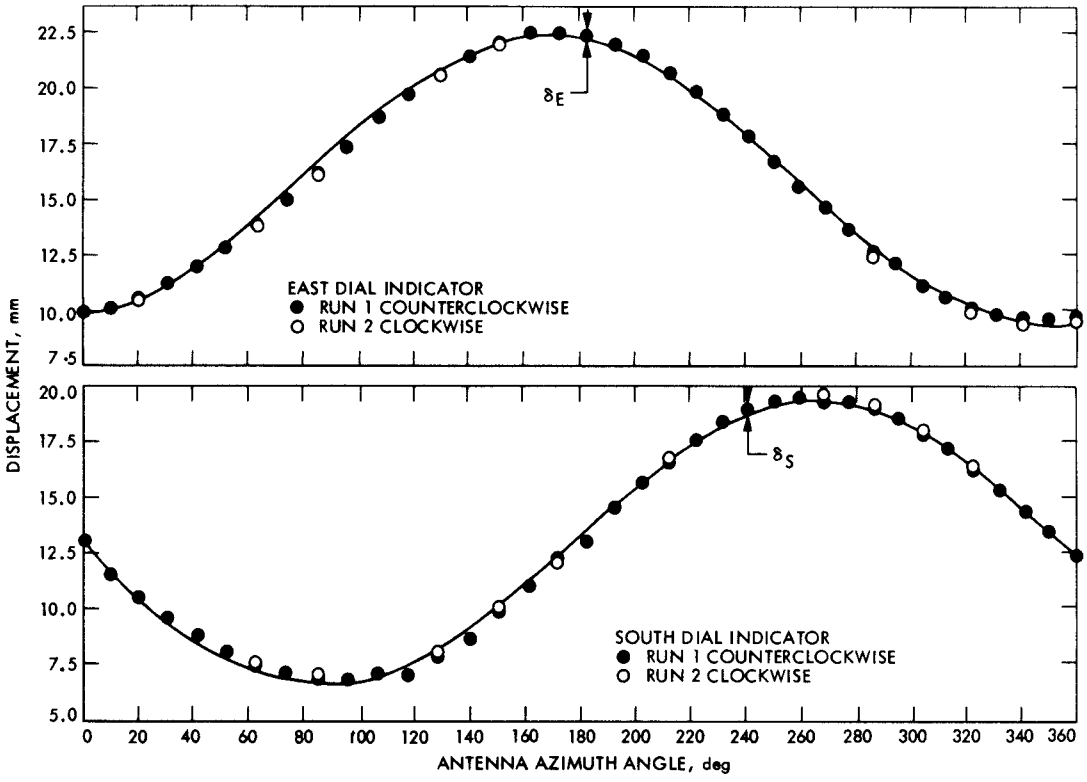

Fig. 3. Dial indicator displacements versus azimuth angle

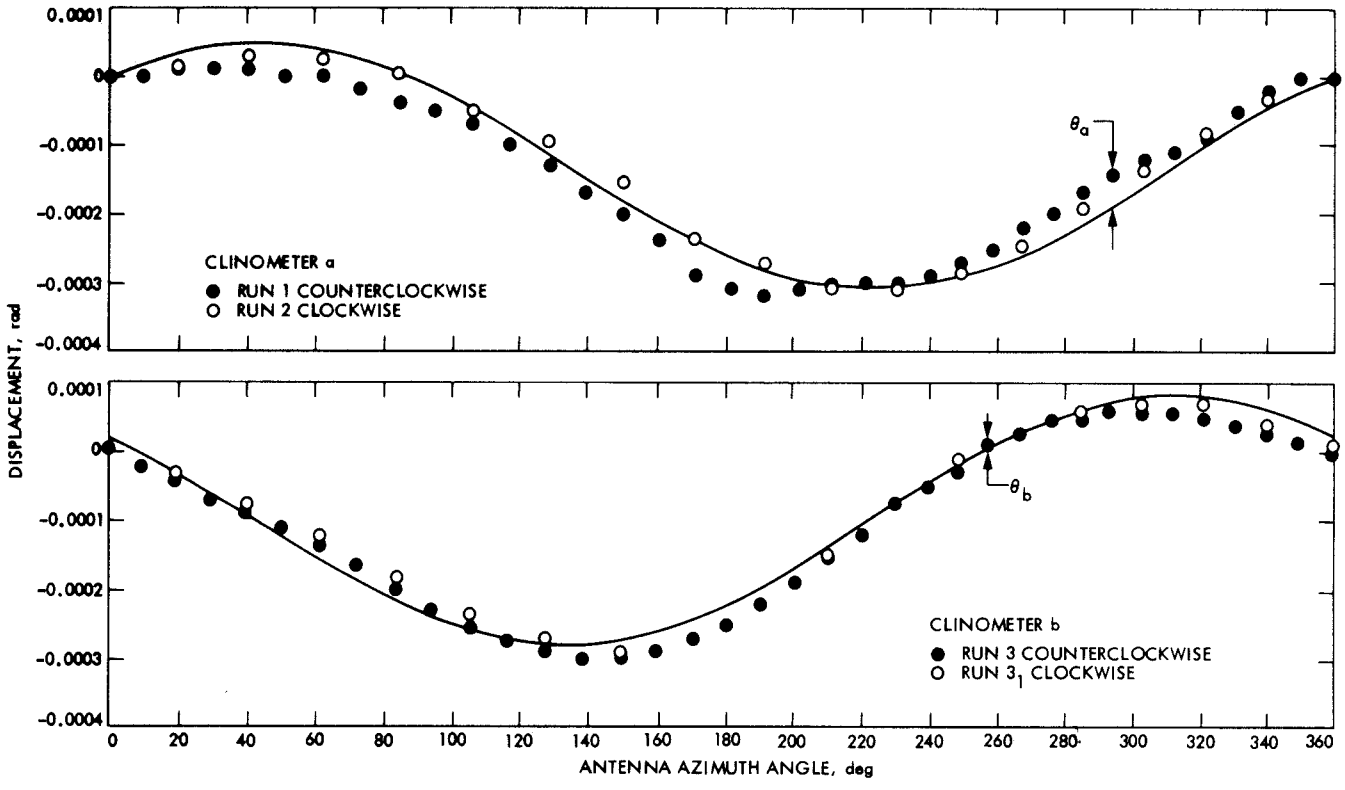

Fig. 4. Angles Θ_a and Θ_b versus azimuth angle

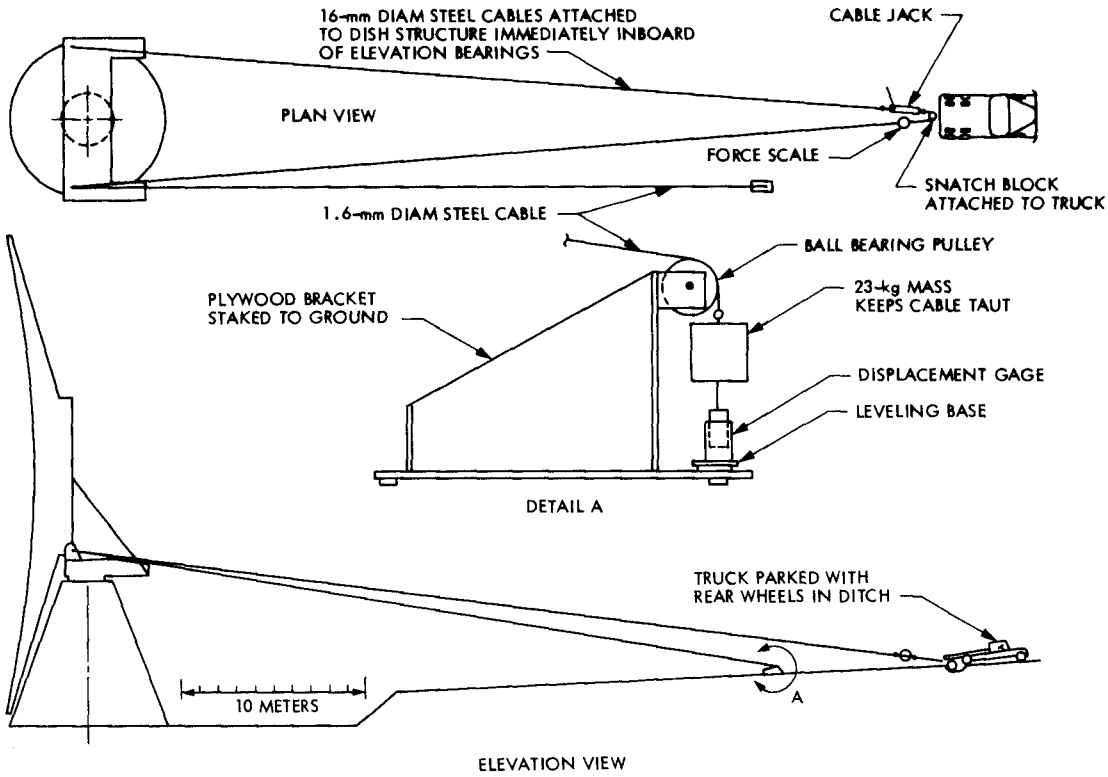

Fig. 5. Configuration of pull-displacement test

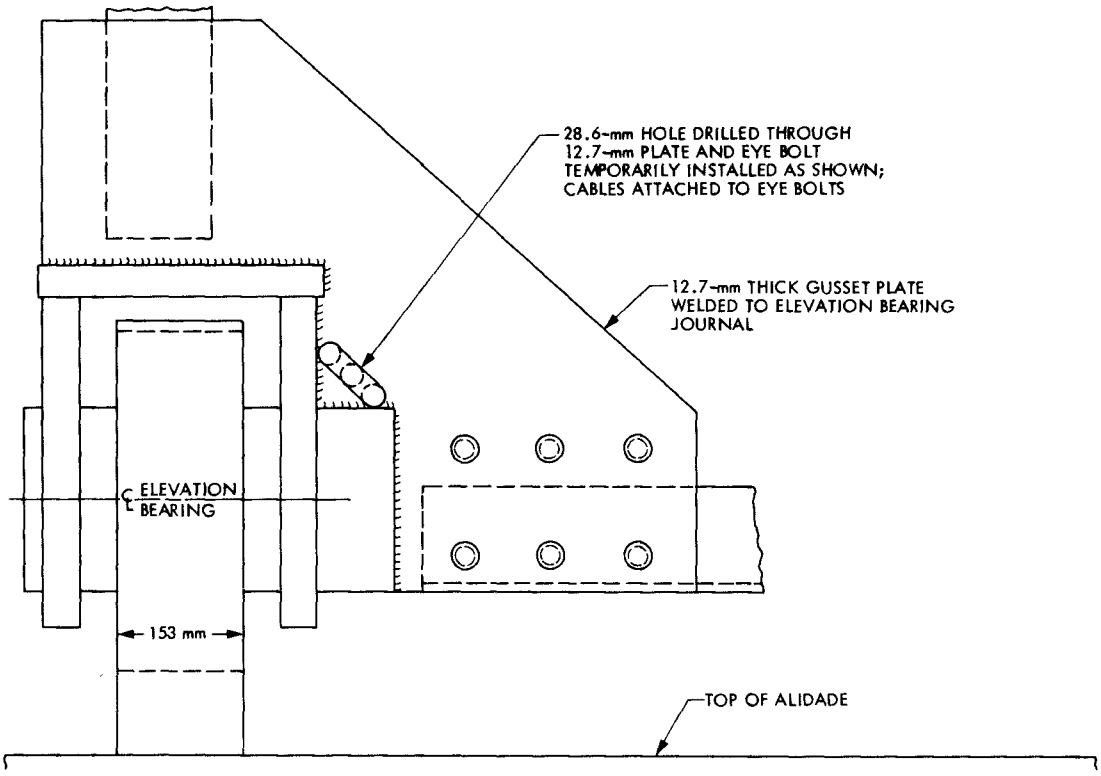

Fig. 6. Method of attaching cables near elevation bearings

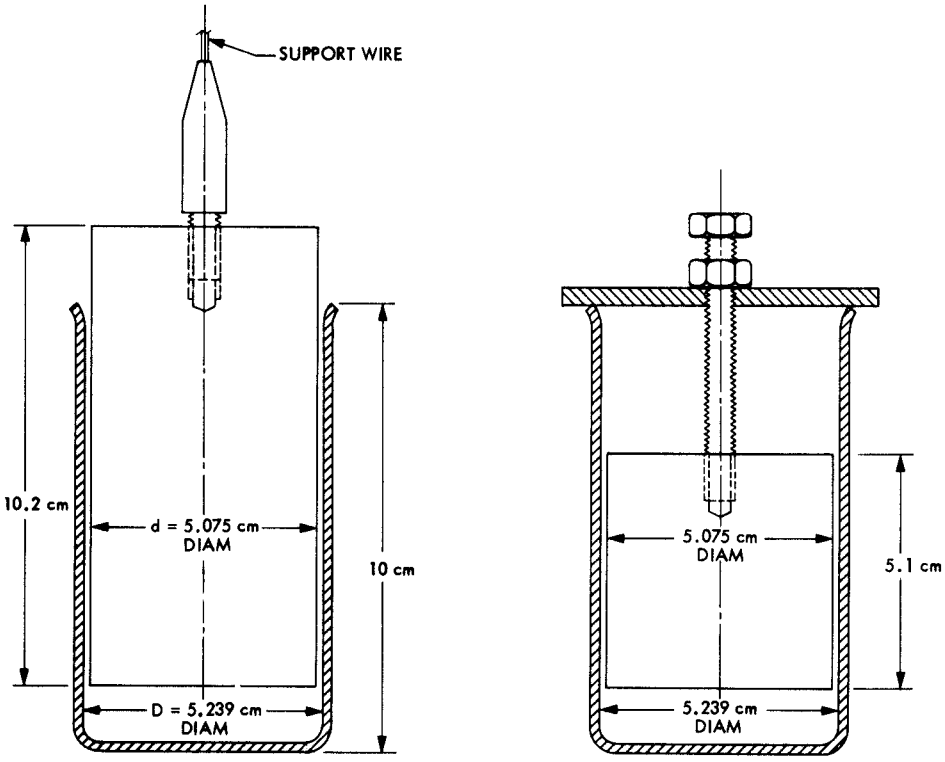

Fig. 7. Details of displacement gages

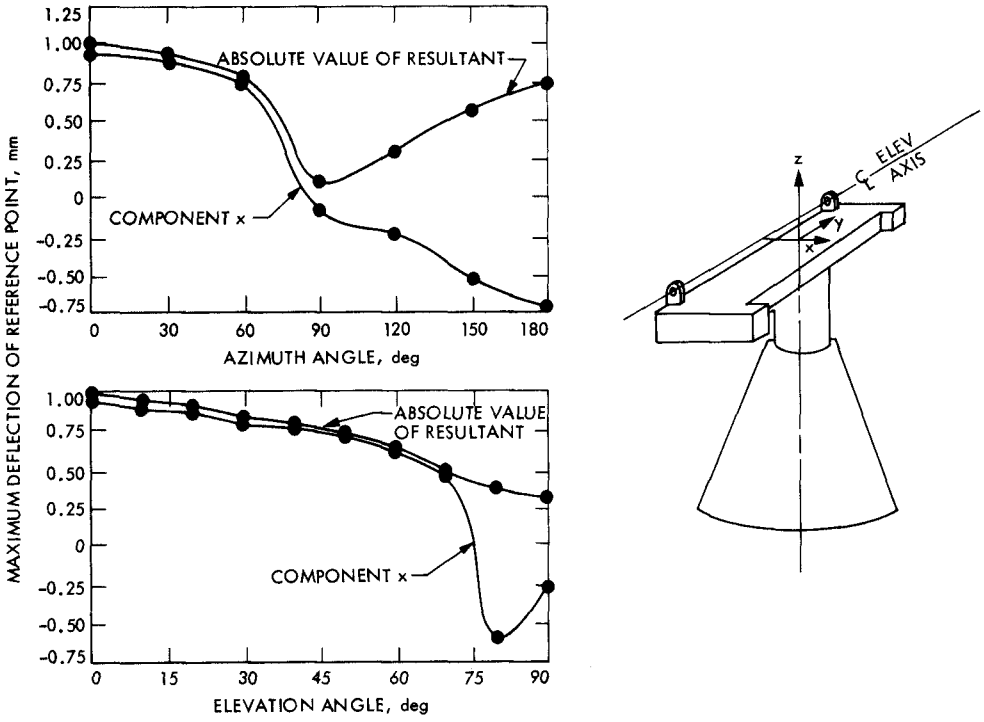

Fig. 8. Deflection of DSS 13 26-m antenna reference point in 14.14-m/s wind

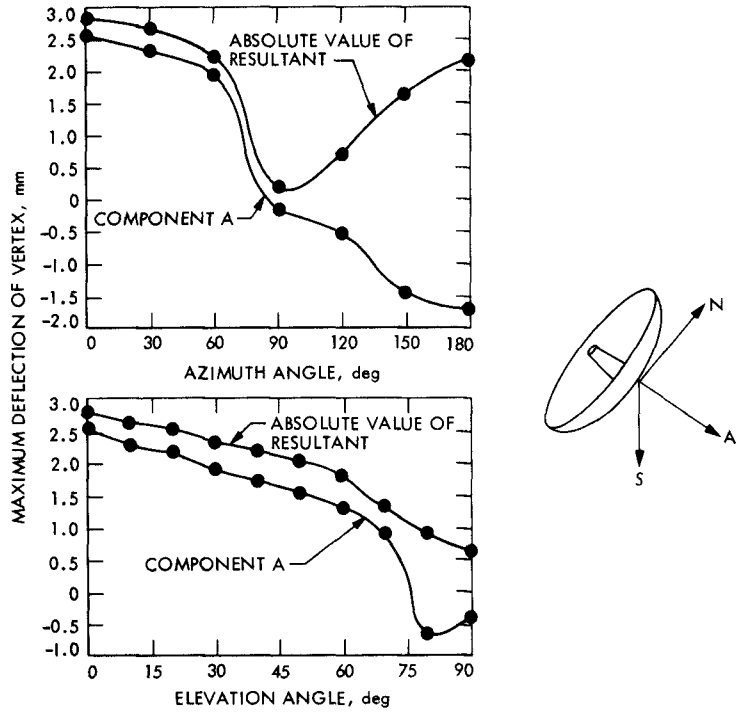

Fig. 9. Deflection of DSS 13 26-m antenna vertex in 14.14-m/s wind

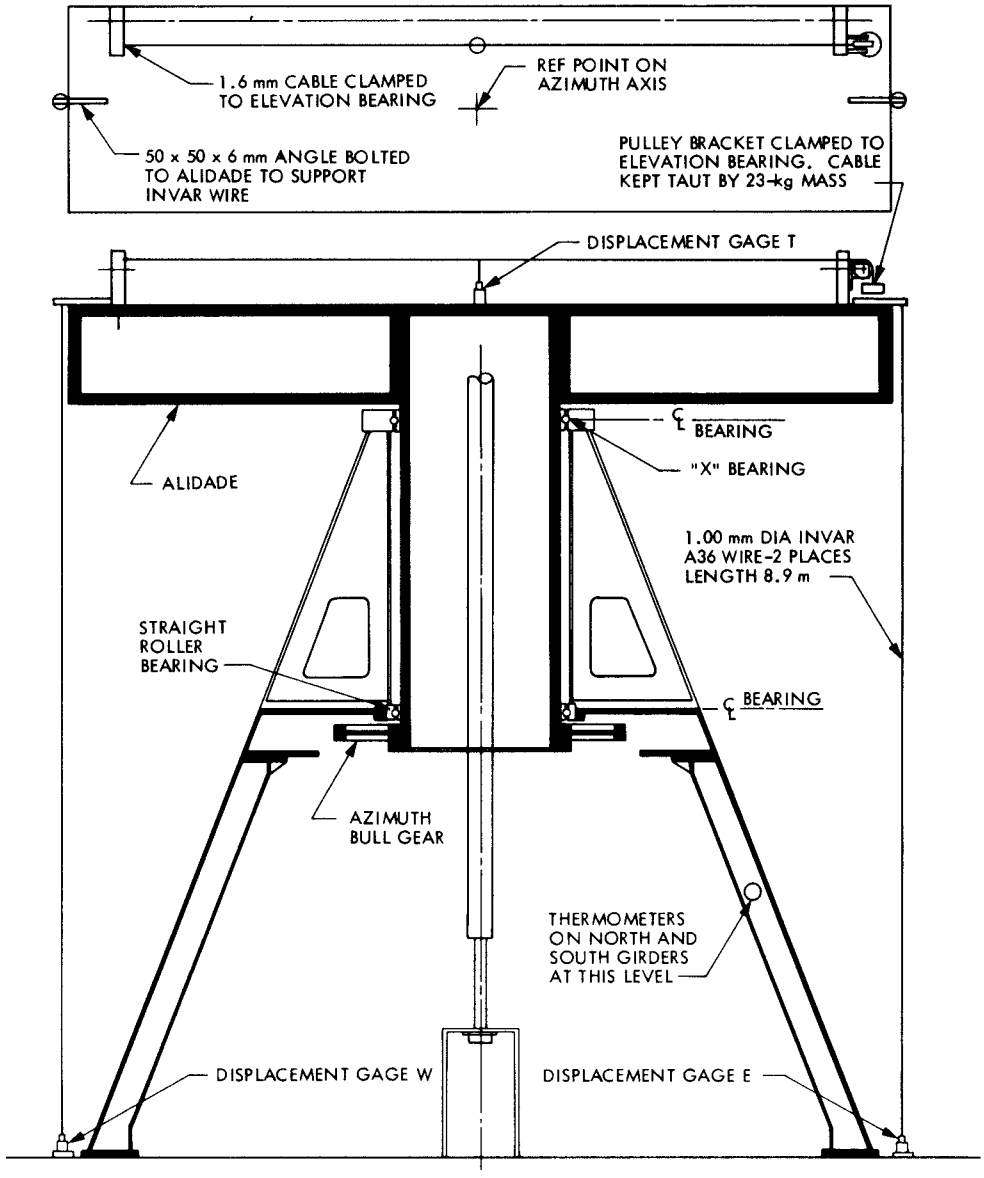

Fig. 10. Vertical motion instrumentation

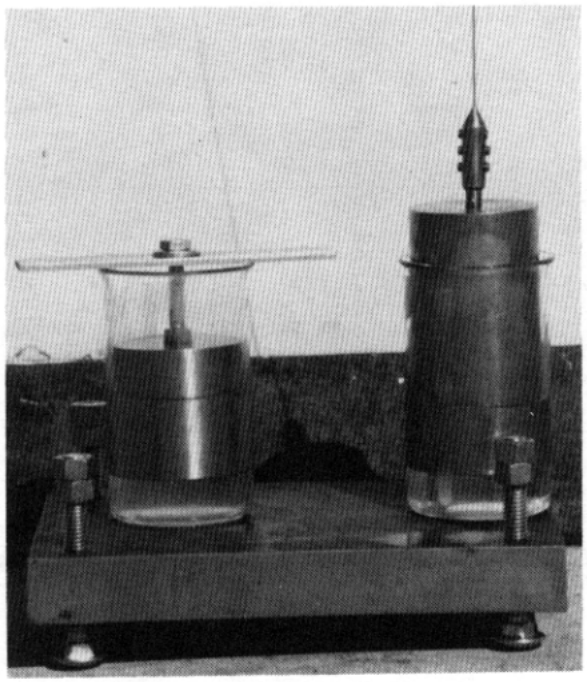

Fig. 11. Photograph of dummy and active displacement gages

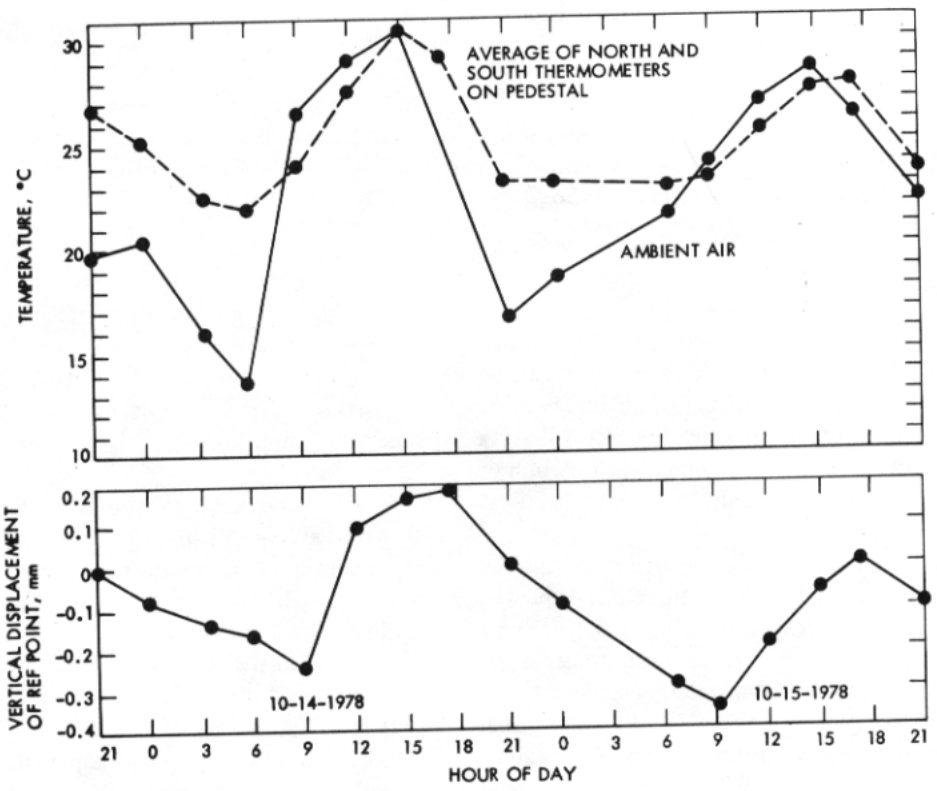

Fig. 12. Vertical displacement of reference point caused by temperature changes